
Rotation-Invariant Local-to-Global Representation Learning for 3D Point Cloud

Seohyun Kim^{1,2}Jaeyoo Park²Bohyung Han²¹NAVER LABS²Computer Vision Lab. & ASRI, Seoul National University¹seo.kkkm@naverlabs.com ²{bellos1203, bhan}@snu.ac.kr

Abstract

We propose a local-to-global representation learning algorithm for 3D point cloud data, which is appropriate to handle various geometric transformations, especially rotation, without explicit data augmentation with respect to the transformations. Our model takes advantage of multi-level abstraction based on graph convolutional neural networks, which constructs a descriptor hierarchy to encode rotation-invariant shape information of an input object in a bottom-up manner. The descriptors in each level are obtained from neural networks based on graphs via stochastic sampling of 3D points, which is effective to make the learned representations robust to the variations of input data. The proposed algorithm presents the state-of-the-art performance on the rotation-augmented 3D object recognition benchmarks and we further analyze its characteristics through comprehensive ablative experiments.

1 Introduction

3D object recognition based on point cloud data has witnessed remarkable achievement in recent years thanks to deep learning technologies [1–10]. While sparse and irregular structures and missing and noisy information of 3D point cloud data have been addressed actively using deep neural networks, geometric transformations remain challenging problems and transformation-invariant representation learning requires a more principled formulation. Among many geometric transformations, rotation is particularly difficult to handle in practice and existing algorithms often rely on the assumption of upright object poses. One of the straightforward solutions to address this issue without the prior is data augmentation, but it is not trivial to cover all possible rotations and generalize on realistic examples due to high computational cost and unexpected corner cases.

There exist a handful of techniques to tackle geometric transformations of 3D point cloud data in the context of 3D object recognition. For example, [1, 2] canonicalize input point coordinates using a spatial transform network, but they require data augmentation to work consistently on the variable transformation of input examples. More recent works [11–14] attempt to employ handcrafted transformation-invariant features such as distances and angles for robust recognition. Although these approaches present practical performance gains, such low-level geometric features have limited capability to express detailed shape information and their computation suffers from an asymptotic increase of computational complexity due to the joint consideration of multiple points.

To address such critical challenges, we introduce a novel rotation-invariant 3D object recognition framework by proposing a descriptor based on the local reference frame (LRF), which is constructed based on a local coordinate system. The receptive field of a descriptor is enlarged stochastically and the generated features are better regularized and representative even with substantial variations of the object shape. Moreover, the proposed method designs the descriptors hierarchically, which provides the capability to represent global rotation-invariant information of a target object effectively. Finally, we utilize graph convolutional neural networks (GCNs) upon stochastically generated graphs based

on progressively encoded local-to-global shape information, which also facilitates the robustness to perturbations and outliers. The source codes are available at our project page¹.

The contributions of this paper are summarized below:

- We introduce a local-to-global representation learning method for 3D point cloud data based on graph convolutional neural networks to model rotation-invariant features in a progressive manner without computing any geometric features, such as angle or distance.
- The proposed algorithm enlarges receptive field sizes and regularizes learned features by computing the descriptors stochastically. This strategy is effective in enhancing robustness to perturbations and outliers.
- Our approach presents great performance improvement on 3D object classification benchmark based on point cloud data, even without data augmentation with respect to rotation.

The rest of the paper is organized as follows. We first discuss existing works about object recognition based on 3D point cloud data in Section 2. Section 3 describes the proposed approach to generate rotation-invariant local descriptors and construct graph convolutional neural networks using the features hierarchically. We present the experimental results on the standard benchmark datasets in Section 4, and make the conclusion in Section 5.

2 Related Works

Deep learning for 3D point cloud recognition On the strength of the prominent advances of deep neural networks, the task of recognizing 3D objects with raw coordinates of inputs has attracted a lot of interest. As a pioneer, [1] proposed PointNet to extract global features from the unordered set of original points. However, PointNet lacks the ability to understand the local feature of an object, which plays a crucial role in various tasks related to 3D objects. Since then, some strategies to learn the local features, such as building a hierarchical model [3] or incorporating edge information [2], give an impressive performance boost on the classification task. However, they still suffer from performance degradation induced by rotated inputs. In our work, we aim to construct the 3D object recognition framework, which is robust to rotation.

Rotation-robust learning for 3D point cloud recognition Designing rotation-robust feature representations is critical to achieve competitive performance in 3D object recognition. In the early days, spatial transform networks (STNs) [1, 2] were employed to provide robustness upon rigid geometric transformations. Then, rotation-equivariant networks [15, 16] based on spherical functions were proposed to improve robustness to rotation. SFCNN [17] proposed an approach to transform the 3D point cloud into an icosahedral lattice. However, all of the aforementioned methods are still vulnerable to unseen orientations and rely heavily on rotation-augmented data to recognize an object successfully. More recent methods often extract geometric features such as distances and angles by considering multiple points jointly; [13] employs the relative angle of the normal vectors and the difference vector of the point pairs. [11] aggregates the information of azimuthal/polar angle and radial distance between two points. Similarly, [12] utilizes the distances and angles among the local triangular structure, which is built upon a reference point, a local neighborhood centroid, and local neighborhood points. However, the manual feature extraction steps, where , in [11–13] may incur the information loss, which induces ambiguities in recognizing an object. For instance, a local triangle and a descriptor in [12] have many-to-one correspondences because a point is expressed in terms of distances and angles with respect to two reference points, which means the point defines a circular trace. On the contrary, we adopt a local reference frame to attain rotation-invariant local descriptors, where the model maintains shape information and aggregates those local descriptors hierarchically to obtain global features. Moreover, our model takes the original 3D points and, consequently, is free from information loss.

Graph-based networks for 3D point cloud tasks Graph convolutional neural networks (GCNs) have made a lot of progress in the past decade [18–21] and achieved great success on many machine learning tasks. The graph-based approaches are often categorized into two groups: 1) ones considering spatial structure and 2) ones based on spectral graph theory. Generally, the cases based on the spatial

¹https://cv.snu.ac.kr/research/rotation_invariant_12g/

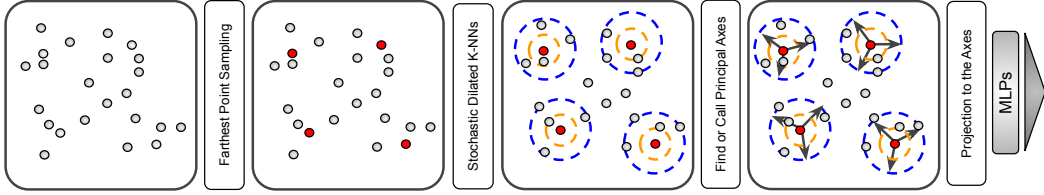


Figure 1: Illustration of descriptor extraction module. Given a set of points, we select a set of representative points (colored in red) using the FPS algorithm. Then, we use the stochastic dilated k -NNs (orange & blue circle) for searching neighbors. Each local region finds the principal axes to be transformed. Then, the transformed regions are mapped into high dimensional features with MLPs.

graphs set their focus on edge information [2, 22, 23]. DGCNN [2] proposed an edge convolution operation and constructed a graph in every layer dynamically to extract local geometric features. ECC [22] proposed an edge-conditioned convolutional network, which generates an edge-specific weight matrix and aggregates neighborhood features spatially. DeepGCNs [23] found out that the spatial graph convolutional layers can be stacked deeply with the residual connections while solving vanishing gradient and over-fitting problem. At the same time, the approaches based on spectral graph theory [18–20] have developed in parallel. [7] constructs a graph structure on the whole 3D point cloud inputs and applies spectral graph filtering with the filter approximated by Chebyshev polynomials [19]. Instead of applying graph convolution for whole point cloud, [4] leverages spectral graph filtering [20] to compute the local descriptors with a hierarchical structure, which shows a better performance than that of using pure multi-layer perceptron layers. However, [4, 7] are still vulnerable to geometric transformation since the graph signal is represented as 3D coordinates. In contrast, we apply approximated spectral graph filtering [20] to the local point features generated in a rotation-invariant manner.

3 Learning Stochastic Rotation-Invariant Representations

3.1 Overview

Our goal is to build a rotation-invariant 3D object recognition framework, which takes an unordered set of point clouds $\mathcal{P} = \{p_1, \dots, p_N\}$ as input, where $p_i \in \mathbb{R}^3$ ($i = 1 \dots N$). In other words, we aim to learn a differentiable function $f : \mathbb{R}^{N \times 3} \rightarrow \mathbb{R}^F$, which satisfies the following property:

$$f(\mathcal{P}) = f(r(\mathcal{P})), \quad (1)$$

where $r : \mathbb{R}^{N \times 3} \rightarrow \mathbb{R}^{N \times 3}$ is an arbitrary $\text{SO}(3)$ rotation mapping function.

Our framework consists of three modules, *descriptor extraction*, *descriptor extension* and *graph-based abstraction*. The first one, descriptor extraction, constructs local shape descriptors by stochastically sampling representative points and encoding the points under a corresponding local reference frame using a neural network model. Next, the descriptor extension module expands the scope of each descriptor in a progressive manner and organizes local-to-global representation hierarchies. Finally, in the graph-based abstraction step, GCNs are employed to acquire context-aware feature representations by incorporating neighboring descriptors.

3.2 Descriptor Extraction

This module aims to learn a set of local descriptors using representative points and their neighboring points. To obtain such robustness, the neighboring points are projected onto a local reference frame (LRF) by the principal component analysis built upon the local region. This idea is motivated by the observation that the descriptors in a local region are not largely affected by rotations with respect to a global coordinate system. Figure 1 illustrates an overview of this module.

The first step of the module is to identify representative points and locate their neighbors. We select a set of representative points $\mathcal{Q} = \{q_1, \dots, q_M\} \in \mathbb{R}^{M \times 3} \subset \mathcal{P}$ ($M \ll N$) using the farthest points sampling (FPS) algorithm [24]. Formally, the objective function of the FPS algorithm is

$$\max_{p \in \mathcal{P}} \min_{q \in \mathcal{Q}} \text{dist}(p, q), \quad (2)$$

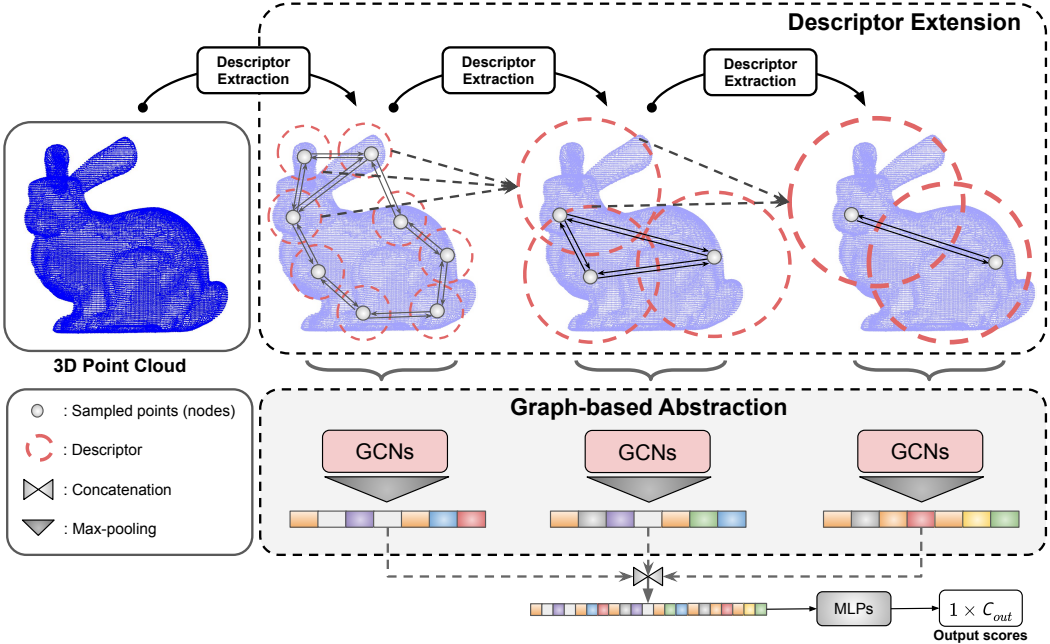


Figure 2: The proposed network architecture for rotation-invariant 3D object classification. Descriptor extension has multiple stacks of the descriptor extraction module, which expands the scope of descriptors by grouping the local features while maintaining rotation invariance. Graph-based abstraction aggregates local descriptors with graph convolutional neural networks by constructing their topological structure at each hierarchy.

where $\text{dist}(\cdot, \cdot)$ is a metric distance function. Although the problem of identifying the optimal \mathcal{Q} is NP-Hard, we can approximate the solution by iteratively finding the farthest point at every stage in a greedy manner until the number of the selected points reaches M . This solution is known as a 2-approximation algorithm.

Each representative point q_i ($i = 1 \dots M$) defines a local region by searching for its neighbors from the original point set \mathcal{P} . Here, to handle large variations in shape, we employ a stochastic version of the recently proposed dilated k -NN search [23]. Given an anchor point q_i and a dilation rate d , the output of the dilated k -NN search is an index set of k points in \mathcal{P} , which are located at every d -th position in the sorted list of the distances from q_i . We add stochasticity to the dilated k -NN search by setting both k and d as random variables during training, which has strong regularization effects and improves the performance of the framework.

Next, we construct a local reference frame based on each q_i and its neighbors. As shown in Figure 1, we adopt two local point sets, $\mathcal{N}_{k,1}(q_i)$ (orange circle) and $\mathcal{N}_{k,d}(q_i)$ (blue circle), with respect to each anchor point q_i using two different search scopes. Note that the dilation rate of $\mathcal{N}_{k,1}(q_i)$ is set to 1 while that of $\mathcal{N}_{k,d}(q_i)$ is a random variable d . The local reference frame is obtained by principal component analysis using the points in $\mathcal{N}_{k,d}(q_i)$, which are then projected onto the estimated reference frame. We denote the projected set of points as $\mathcal{N}'_{k,d}(q_i)$.

The last step of this module generates the local descriptors based on the rotation-normalized information in the local reference frame. The descriptor corresponding to q_i , denoted by $\phi_i \in \mathbb{R}^C$, is obtained by

$$\phi_i = f_\Theta([g_1(\mathcal{N}'_{k,1}(q_i)), g_2(\mathcal{N}'_{k,d}(q_i))]), \quad (3)$$

where $f_\Theta(\cdot)$, $g_1(\cdot)$ and $g_2(\cdot)$ are multi-layer perceptrons followed by max pooling layers, and $[\cdot, \cdot]$ denotes tensor concatenation in the channel direction.

3.3 Descriptor Extension

Suppose that we are given a set of points and their descriptors, $\mathcal{Q} = \{q_1, \dots, q_M\}$ and $\mathcal{H} = \{\phi_1, \dots, \phi_M\}$, by the descriptor extraction module. Then, the first level of the descriptor extension module takes those two sets, $\mathcal{Q}_0 \equiv \mathcal{Q}$ and $\mathcal{H}_0 \equiv \mathcal{H}$, as its inputs and produces the same type of sets for the input of the subsequent level, \mathcal{Q}_1 and \mathcal{H}_1 , where $|\mathcal{Q}_1| \ll |\mathcal{Q}_0|$. The descriptor extension module repeat this procedure for a predefined number of iterations.

Basically, the procedure in the descriptor extension module is almost identical to the descriptor extraction module, but they have the following differences. First, each level of this module deals with a reduced number of points by applying the farthest point sampling, which also updates local point sets. Second, in each level of this module, $g_2(\mathcal{N}'_{k,d}(q_i))$ in Eq. (3) is replaced by the descriptor representation obtained from the previous level, *e.g.*, ϕ_i . Third, we reuse the principal axes obtained from the descriptor extraction module, rather than recompute them in each level. That is because, as hierarchy goes deeper, points become sparser and the newly obtained axes would not be stable.

In a nutshell, this module constructs a hierarchical structure to extend coverage of the local descriptors obtained from the descriptor extraction module and elevates the semantic levels of the descriptors with the extended scopes. This is achieved by aggregating the information in nearby features, which facilitates local geometry understanding over a wider area and saves computational cost by reducing the size of GCNs, both in a progressive fashion. Note that it is highly desirable to enlarge the scope of the descriptors since local shapes can be identified and characterized effectively with large receptive fields. Figure 2 illustrates the pipeline of our description extension module.

3.4 Graph-based Abstraction

The objective of the graph-based abstraction module is to obtain context-aware descriptors by referring to the connectivity among the descriptors. Since the information learned at each hierarchy so far is merely the partial shape of an object, it is desirable for each descriptor to be aware of its geometric context to better understand the overall shape. In order to aggregate the information of the descriptors, we apply GCNs at the end of each level. Moreover, the graphs are built stochastically to cover the various scopes and learn diverse contexts.

More specifically, the descriptors at each level are first converted to the graph signal $X_l \in \mathbb{R}^{n_l \times c_l}$, where n_l is the number of the nodes and c_l is the feature dimension at the l -th hierarchy. For simplicity, we omit the index l for the rest of the section. For the adjacency matrix $A \in \mathbb{R}^{n \times n}$, we construct a k -NN graph while setting the number of edges to the neighbors as a random variable \hat{k} . We weigh the edges between the nodes as the Euclidean distance smoothed by a Gaussian kernel.

Based on the constructed graph, we adopt GCNs following [20], which introduces a renormalization trick to approximate the graph as $\hat{A} = \tilde{D}^{-\frac{1}{2}} \tilde{A} \tilde{D}^{-\frac{1}{2}}$, where $\tilde{A} = A + I_n$ is the adjacency matrix with self-connections, and $\tilde{D}_{ii} = \sum_j \tilde{A}_{ij}$ is a degree matrix. Then, GCNs are applied to enhance the representational power of X as

$$Y = \text{ReLU} \left(\hat{A} X W \right), \quad (4)$$

where W is a learnable parameter matrix. As illustrated in Figure 2, the outputs from all of the hierarchies are max-pooled and are concatenated to obtain the final representation for classification.

4 Experiments

This section presents the experimental results of our algorithm compared to existing approaches. We demonstrate the effectiveness of our framework via several ablation studies. The evaluation protocol in this paper is identical to those conducted in previous works [11, 12, 16, 17]. Specifically, we perform experiments in three modes: training and testing with azimuthal rotations (z/z), training with azimuthal rotations and testing with arbitrary rotations ($z/\text{SO}(3)$), and training and testing with arbitrary rotations ($\text{SO}(3)/\text{SO}(3)$).

Table 1: 3D object classification results on ModelNet40. The column located in the last, Drop, shows the performance difference of SO(3)/SO(3) and z/SO(3).

Method	Input (dimensionality)	z/z (%)	z/SO(3) (%)	SO(3)/SO(3) (%)	Drop
PointNet (w/o STN) [1]	pc (1024 x 3)	88.5	16.4	70.5	54.1
PointNet++ (MSG w/o STN) [3]	pc+normal (5000 x 6)	91.9	18.4	74.7	56.3
SO-Net (w/o STN) [25]	pc+normal (5000 x 6)	93.4	19.6	78.1	58.5
DGCNN (w/o STN) [2]	pc (1024 x 3)	91.2	16.2	75.3	59.1
PointNet [1]	pc (1024 x 3)	89.2	16.2	75.5	59.3
PointNet++ [3]	pc+normal (5000 x 6)	91.8	18.4	77.4	59.0
SO-Net [25]	pc+normal (5000 x 6)	91.2	21.1	80.2	59.1
DGCNN [2]	pc (1024 x 3)	92.2	20.6	81.1	60.5
SpecGCN [4]	pc (1024 x 3)	91.5	28.8	75.3	46.5
Spherical CNN [16]	Voxel (2 x 64 x 64)	88.9	76.9	86.9	10.0
SFCNN [17]	pc (1024 x 3)	91.4	84.8	90.1	5.3
SFCNN [17]	pc+normal (1024 x 6)	92.3	85.3	91.0	5.7
RICConv [12]	pc (1024 x 3)	86.5	86.4	86.4	0.0
ClusterNet [11]	pc(1024 x 3)	87.1	87.1	87.1	0.0
Ours	pc (1024 x 3)	89.5	89.5	89.5	0.0
Ours (with normal)	pc+normal (1024 x 6)	91.0	91.0	91.0	0.0

4.1 Implementation Details

Our model is implemented in Tensorflow and all experiments are conducted on a single NVIDIA Titan XP GPU. The learning rate is 0.001 and batch size is 32. We downsample 256, 128, and 64 points respectively for each descriptor extraction module in our framework. For each hierarchies, the number of searching neighbors of stochastic dilated k -NNs, k , is sampled from different uniform distribution: $\mathcal{U}(32, 96)$, $\mathcal{U}(16, 48)$, and $\mathcal{U}(8, 24)$. The dilation rate of the first descriptor extraction is sampled from $\mathcal{U}(2, 4)$. Meanwhile, the number of edge on constructing a graph for graph convolution, \hat{k} , is sampled from $\mathcal{U}(8, 24)$, $\mathcal{U}(4, 12)$, and $\mathcal{U}(2, 8)$. For evaluation, we set all those parameters to fixed values where k is set to 64, 32, and 16, \hat{k} is set to 16, 8, and 4, respectively along the hierarchies. The dilation rate is set to 3. At inference time, our algorithm requires 0.56 ms for a single forward step with a single point cloud object. The computational cost mostly stems from the computations of PCAs, which are performed on CPU rather than GPU. It would be possible to parallelize their computations on GPU and improve speed.

4.2 Main Results

To evaluate the robustness to rotation, we compare the proposed algorithm with recent 3D object classification approaches on ModelNet40 [26], a widely used benchmark. It consists of CAD models in 40 categories and contains 9,843 and 2,468 shapes for training and testing, respectively. Point clouds are sampled uniformly from vertices and faces of the CAD models. All points are shifted and normalized to fit in a unit sphere.

Table 1 presents the overall performance of 3D object classification techniques in the three modes, including two recent rotation-invariant algorithms [11, 12]. Most approaches [1–3, 16, 25] show great performance in z/z . However, it is noticeable that their performance is significantly degraded in the presence of unseen rotations for inference. Moreover, although arbitrary rotations are employed for data augmentation during the training phase, SO(3)/SO(3), the generalization performance is not fully recovered in most algorithms. Although PointNet [1], PointNet++ [3], SO-Net [25], and DGCNN [2] incorporate a spatial transformer network (STN) to improve accuracy, it turns out that STN is not effective in handling the arbitrary rotations, SO(3), regardless of data augmentation. SpecGCN [4], which utilizes spectral graph filtering to construct local descriptor, is not robust to rotation since the graph signal is identical to 3D coordinates. Meanwhile, although SFCNN [17] achieves competitive accuracy for the rotations exposed during training via data augmentation, it suffers from handling unseen types of rotations, $z/SO(3)$, and presents large gaps with respect to the accuracies in SO(3)/SO(3). The existing techniques that address rotation invariance explicitly [11, 12] maintain their recognition accuracies for unseen types of rotations, but their baseline performance is

Table 2: Contribution of stochastic learning. The checkmark indicates that the parameter is given stochasticity. The parameters, d , k , and \hat{k} , denote the dilation rate, the number of searching neighbors of stochastic dilated k -NNs, and the number of edge on constructing a graph for graph convolution, respectively.

	d	k	\hat{k}	z/SO(3) (%)
Deterministic	-	-	-	87.7
	✓	-	-	88.6
	-	✓	-	88.9
Partially stochastic	-	-	✓	88.0
	✓	✓	-	89.2
	✓	-	✓	89.0
	-	✓	✓	88.9
Fully stochastic	✓	✓	✓	89.5

Table 3: Results of 3D object classification on ModelNet40 for different methodologies. The classification accuracy is reported.

Ablation types	Variations	z/SO(3) (%)	SO(3)/SO(3) (%)
(a) Architectural variations	MLP	89.1	89.2
	GCN (ours)	89.5	89.5
(b) Transformation scope	Global transformation	87.2	87.2
	Local transformations (ours)	89.5	89.5
(c) Levels of models	Single level	88.7	88.9
	Two levels	89.1	89.3
	Three levels (ours)	89.5	89.5
	Four levels	89.3	89.4
(d) Stochastic dilation	Deterministic dilated k -NN [23]	88.3	88.3
	Stochastic Dilated k -NN (ours)	89.5	89.5

not satisfactory. Our algorithm demonstrates the state-of-the-art accuracy consistently for all cases and robustness to unseen types of rotations.

4.3 Ablation Study

We perform several ablation studies on ModelNet40 to analyze the effectiveness of the proposed approach.

Benefit of stochastic learning To show the effectiveness of stochastic learning, we analyze the impact of three stochastic factors to learn the descriptors—dilation rate d , number of nearest neighbors K , and number of edges for the construction of a graph \hat{k} —and compare the results with the one given by a deterministic approach. Table 2 presents that the model from pure deterministic learning has the lowest accuracy and adding stochastic learning components improves results consistently.

Graph convolutional networks (GCNs) vs. multi-layer perceptrons (MLPs) Table 3 (a) presents the comparison between GCNs and MLPs for recognition models. For comparison, we replace a single GCNs layer with a single fully-connected layer for all hierarchies, where the dimension of the learnable parameter is consistent with GCNs. The use of GCNs in our framework achieves better performance than that of MLPs. This is mainly because GCNs help capture the geometric context since they consider the neighbor features of a single node.

Comparison between local and global transformations We analyze the benefit of feature learning based on local transformations compared to the universal global rotation. To this end, we train a new model identical to ours, except that all 3D points in \mathcal{P} are transformed by a global rotation matrix estimated by a principal component analysis. All the hyperparameters for network configuration and model training are identical to our algorithm based on local transformations. Table 3 (b) presents that

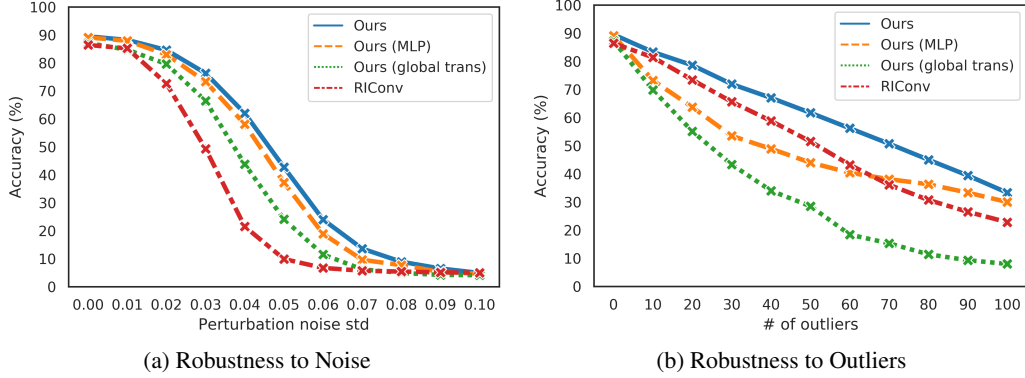


Figure 3: Perturbation and outlier robustness test on ModelNet40. The experiment of (a) is done by adding Gaussian noise for each point along with the different standard deviation and (b) is done with inserting outliers that are sampled inside the unit sphere. Note that all other aspects of the training process of the model with global transformation are consistent with our original framework.

the proposed method based on local coordinate systems outperforms the model based on the global transformation.

Effectiveness of hierarchical modeling To demonstrate the effectiveness of the proposed hierarchical representations, we evaluate classification accuracy with respect to the number of levels in our neural network architecture. Table 3 (c) presents that the enlarging the receptive field of a descriptor using multiple levels improves accuracy gradually while adding more levels is not particularly helpful.

Impact of stochastic dilation in k -NN search Contrary to [23], the proposed algorithm employs a stochastic dilated k -NN search by setting k and d as random variables. In this way, the scope of the nearest neighbor search, $k * d$, is determined stochastically, which regularizes the local descriptors and make the learned model robust to noise and shape variation. Table 3 (d) clearly illustrates the effectiveness of stochastic dilation in our nearest neighbor search strategy.

4.4 Robustness to Noise and Outliers

We also conduct experiments for evaluating robustness to noise in input data: perturbations and outliers. To this end, each input point is perturbed by adding noise from zero-mean normal distributions, $N(0, \sigma^2)$ while outliers sampled from a unit sphere are injected to existing points for each object instance. Note that each object is composed of 1,024 3D points in all compared algorithms.

Figure 3 (a) illustrates the curves with respect to the level of perturbation, and the robustness to perturbation of the proposed algorithm based on GCNs. The use of MLPs instead of GCNs degrades performance marginally in the whole perturbation levels while the global transformation is not effective compared to the local counterpart. One of the state-of-the-art rotation-invariant approach, RICconv [12], suffers from substantial accuracy drop for this kind of noise type.

On the other hand, Figure 3 (b) shows the performance in the presence of outliers, where our full algorithm shows outstanding performance compared to all other methods. In particular, GCN achieves significant accuracy gain compared to MLP. In this case, the local transformations turn out to be better than the global one, which indicates that outlier injection distorts global shape and orientation information more significantly than the local one. For the last, the result of RICconv [12] implies that the representation learning with the lower-level feature is not robust enough to perturbation noise as well as outliers.

4.5 Qualitative Results

Figure 4 presents the examples of graphs that are generated along the hierarchies. The graph at the first level is densely nested and becomes sparser as the hierarchy grows. In this way, as a hierarchy goes deeper, the overall skeleton of the object is captured, which helps extract global representation.

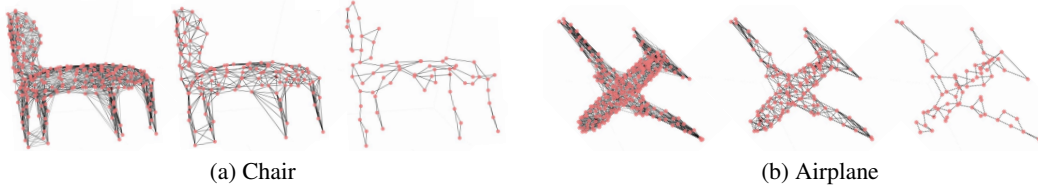


Figure 4: Qualitative examples of generated graphs in all three levels. Circles in red indicate the nodes and solid line means the edge between the nodes.

Table 4: 3D part segmentation results on ShapeNet. The column located in the last, Drop, shows the performance difference of $SO(3)/SO(3)$ and $z/SO(3)$.

Method	Input (dimensionality)	$z/SO(3)$ (%)	$SO(3)/SO(3)$ (%)	Drop
PointNet [1]	pc (1024 x 3)	37.8	74.4	36.6
PointNet++ [3]	pc+normal (5000 x 6)	48.2	76.7	28.5
DGCNN [2]	pc (1024 x 3)	37.4	73.3	35.9
RICconv [12]	pc (1024 x 3)	75.3	75.5	0.2
Ours	pc (1024 x 3)	77.2	77.3	0.1

Thus, the learned representations from the GCNs at multiple levels are complementary to one another in their semantic levels. We demonstrate more qualitative results for the classification task in the supplementary material with the comparison to other methods.

4.6 3D Part Segmentation

We conduct an additional experiment of part segmentation, where the task aims to predict a part label for each point, on ShapeNet [27], following [12]. The dataset consists of 16,881 shapes from 16 object categories with 50 part labels in total. We adopt hierarchical point feature propagation strategy proposed by PointNet++ [3] to obtain upsampled feature map, where all original points have their corresponding point features. Table 4 illustrates the overall performance of 3D part segmentation methods in $z/SO(3)$ and $SO(3)/SO(3)$ mode. The results present that the proposed method is also effective to part segmentation and outperforms the state-of-the-art, especially in the $z/SO(3)$ scenario with the smallest drop rate, which empirically demonstrates that the proposed method handles the arbitrary rotation well.

5 Conclusion

We proposed a novel framework for 3D object classification, which learns rotation-invariant local descriptors based on local reference frames and performs graph convolutional neural networks properly upon topological structure to aggregate local features. Our stochastic learning strategy regularizes the geometric features of 3D objects, which improves performance substantially. Our method directly uses raw point cloud without conversion to lower-level feature, which has been the only proposed solution for rotation invariant 3D object classification task. Also, graph convolutional neural networks equipped with hierarchical structure successfully draw a global descriptor by combining neighboring local features, achieving the state-of-the-art performance on rotation-augmented 3D object classification benchmark. Finally, the extensive experiments in various settings validate the effectiveness of our framework.

Broader Impact

The major goal of our research is to enhance the 3D object recognition framework by imposing the ability to handle rotation transformation. 3D object recognition is applicable to various vision system, such as autonomous driving or augmented reality. From the ethical point of view, the improvement of the 3D object recognition system has both bright and dark sides. On one hand, such a system could benefit those who are visually impaired using auxiliary vision systems including smart glasses [28]. Meanwhile, one can think that the technology might harm personal privacy in the case that the surveillance system equipped with such technology *e.g.* drones [29], closed-circuit TV [30] might achieve powerful recognition ability. Therefore, the academic community should concern the possible privacy issue through the research [31].

References

- [1] Qi, C.R., Su, H., Mo, K., Guibas, L.J.: Pointnet: Deep learning on point sets for 3D classification and segmentation. In CVPR. (2017)
- [2] Wang, Y., Sun, Y., Liu, Z., Sarma, S.E., Bronstein, M.M., Solomon, J.M.: Dynamic graph cnn for learning on point clouds. ACM Transactions on Graphics (TOG) **38**(5) (2019) 146
- [3] Qi, C.R., Yi, L., Su, H., Guibas, L.J.: Pointnet++: Deep hierarchical feature learning on point sets in a metric space. In NIPS. (2017)
- [4] Wang, C., Samari, B., Siddiqi, K.: Local spectral graph convolution for point set feature learning. In ECCV. (2018)
- [5] Atzmon, M., Maron, H., Lipman, Y.: Point convolutional neural networks by extension operators. In SIGGRAPH. (2018)
- [6] Xu, Y., Fan, T., Xu, M., Zeng, L., Qiao, Y.: SpiderCNN: Deep learning on point sets with parameterized convolutional filters. In ECCV. (2018)
- [7] Zhang, Y., Rabbat, M.: A graph-cnn for 3D point cloud classification. In ICASSP. (2018)
- [8] Xiong, Y., Ren, M., Liao, R., Wong, K., Urtasun, R.: Deformable filter convolution for point cloud reasoning. arXiv preprint arXiv:1907.13079 (2019)
- [9] Thomas, H., Qi, C.R., Deschaud, J.E., Marcotegui, B., Goulette, F., Guibas, L.J.: KPConv: Flexible and deformable convolution for point clouds. In ICCV. (2019)
- [10] Wu, W., Qi, Z., Fuxin, L.: PointConv: Deep convolutional networks on 3D point clouds. In CVPR. (2019)
- [11] Chen, C., Li, G., Xu, R., Chen, T., Wang, M., Lin, L.: ClusterNet: Deep hierarchical cluster network with rigorously rotation-invariant representation for point cloud analysis. In CVPR. (2019)
- [12] Zhang, Z., Hua, B.S., Rosen, D.W., Yeung, S.K.: Rotation invariant convolutions for 3D point clouds deep learning. In International Conference on 3D Vision (3DV). (2019)
- [13] Deng, H., Birdal, T., Ilic, S.: PPF-FoldNet: Unsupervised learning of rotation invariant 3D local descriptors. In ECCV. (2018)
- [14] Deng, H., Birdal, T., Ilic, S.: PPFNet: Global context aware local features for robust 3D point matching. In CVPR. (2018)
- [15] Cohen, T.S., Geiger, M., Köhler, J., Welling, M.: Spherical CNNs. In ICLR. (2018)
- [16] Esteves, C., Allen-Blanchette, C., Makadia, A., Daniilidis, K.: Learning SO (3) equivariant representations with spherical cnns. In ECCV. (2018)
- [17] Rao, Y., Lu, J., Zhou, J.: Spherical fractal convolutional neural networks for point cloud recognition. In CVPR. (2019)
- [18] Bruna, J., Zaremba, W., Szlam, A., LeCun, Y.: Spectral networks and locally connected networks on graphs. In ICLR. (2014)
- [19] Defferrard, M., Bresson, X., Vandergheynst, P.: Convolutional neural networks on graphs with fast localized spectral filtering. In NIPS. (2016)
- [20] Kipf, T.N., Welling, M.: Semi-supervised classification with graph convolutional networks. In ICLR. (2017)
- [21] Hammond, D.K., Vandergheynst, P., Gribonval, R.: Wavelets on graphs via spectral graph theory. Applied and Computational Harmonic Analysis **30**(2) (2011) 129–150
- [22] Simonovsky, M., Komodakis, N.: Dynamic edge-conditioned filters in convolutional neural networks on graphs. In CVPR. (2017)

- [23] Li, G., Müller, M., Thabet, A., Ghanem, B.: DeepGCNs: Can GCNs Go as Deep as CNNs? In ICCV. (2019)
- [24] Gonzalez, T.F.: Clustering to minimize the maximum intercluster distance. *Theoretical Computer Science* **38** (1985) 293–306
- [25] Li, J., Chen, B.M., Hee Lee, G.: SO-Net: Self-organizing network for point cloud analysis. In CVPR. (2018)
- [26] Wu, Z., Song, S., Khosla, A., Yu, F., Zhang, L., Tang, X., Xiao, J.: 3D shapenets: A deep representation for volumetric shapes. In CVPR. (2015)
- [27] Chang, A.X., Funkhouser, T., Guibas, L., Hanrahan, P., Huang, Q., Li, Z., Savarese, S., Savva, M., Song, S., Su, H., Xiao, J., Yi, L., Yu, F.: ShapeNet: An Information-Rich 3D Model Repository. arXiv preprint arXiv:1512.03012 (2015)
- [28] Zhao, Y., Hu, M., Hashash, S., Azenkot, S.: Understanding low vision people's visual perception on commercial augmented reality glasses. In CHI(Conference on Human Factors in Computing Systems). (2017)
- [29] Finn, R.L., Wright, D.: Privacy, data protection and ethics for civil drone practice: A survey of industry, regulators and civil society organisations. *Computer Law & Security Review* **32**(4) (2016) 577–586
- [30] Senior, A., Pankanti, S., Hampapur, A., Brown, L., Tian, Y.L., Ekin, A., Connell, J., Shu, C.F., Lu, M.: Enabling video privacy through computer vision. *IEEE Security & Privacy* **3**(3) (2005) 50–57
- [31] Speciale, P., Schonberger, J.L., Kang, S.B., Sinha, S.N., Pollefeys, M.: Privacy preserving image-based localization. In CVPR. (2019)

Rotation-Invariant Local-to-Global Representation Learning for 3D Point Cloud

Supplementary Material

Seohyun Kim^{1, 2}

Jaeyoo Park²

Bohyung Han²

¹NAVER LABS

²Computer Vision Lab. & ASRI, Seoul National University

¹seo.kkkm@naverlabs.com ²{bellos1203, bhan}@snu.ac.kr

1 Additional Qualitative Results

Table 1 illustrates additional qualitative results for the 3D point cloud classification task. Here, we present the predictions of other models [1, 2, 3, 4, 5] for the rotated inputs from ModelNet40. All of the frameworks are trained with the data augmented by azimuthal rotation only (z/SO3). In (a) and (b), PointNet [1], PointNet++ [2], DGCNN [3], the frameworks equipped with a spatial transformer network (STN), and SpecGCN [4] are not able to handle the rotated inputs. Although RICConv [5] has the ability to recognize the rotated objects with distinct characteristics, such as wings of airplane or legs of table, (c) and (d) show that RICConv fails to identify a much simpler structure (c) or small distinct parts such as small wheels (d). Especially from (d), we can interpret the result as RICConv [5] might lose local information with small coverage, while our framework retains such local information with the aid of local reference frame, even if the object is rotated. (e) presents the failure case of our model. However, the shape is not much distinctive and it is hard to recognize as Xbox even for the human, and all of the presented models fails.

Table 1: Additional qualitative results on the rotated inputs from ModelNet40. All of the frameworks are trained with the data augmented by azimuthal rotation only (z/SO3).

	GT	PointNet	PointNet++	DGCNN	SpecGCN	RICov	Ours
(a) 	airplane	plant	plant	plant	plant	airplane	airplane
(b) 	table	stairs	door	stool	chair	table	table
(c) 	bowl	plant	vase	vase	plant	tent	bowl
(d) 	car	stairs	bottle	plant	bottle	stairs	car
(e) 	xbox	tv-stand	tent	table	tent	range-hood	radio

References

- [1] Qi, C.R., Su, H., Mo, K., Guibas, L.J.: Pointnet: Deep learning on point sets for 3D classification and segmentation. In CVPR. (2017)
- [2] Qi, C.R., Yi, L., Su, H., Guibas, L.J.: Pointnet++: Deep hierarchical feature learning on point sets in a metric space. In NIPS. (2017)
- [3] Wang, Y., Sun, Y., Liu, Z., Sarma, S.E., Bronstein, M.M., Solomon, J.M.: Dynamic graph cnn for learning on point clouds. ACM Transactions on Graphics (TOG) **38**(5) (2019) 146
- [4] Wang, C., Samari, B., Siddiqi, K.: Local spectral graph convolution for point set feature learning. In ECCV. (2018)
- [5] Zhang, Z., Hua, B.S., Rosen, D.W., Yeung, S.K.: Rotation invariant convolutions for 3D point clouds deep learning. In International Conference on 3D Vision (3DV). (2019)